Line Structured Light Measurement System, Method and Experiments for Rail Profile

Qingli Luo*, Shubin Zhang and Zhiyuan Chen
State Key Laboratory of Precision Measuring Technology and Instruments, Tianjin University, No. 92, Weijin Road, Nankai District, Tianjin 300072, China

Keywords: Line Structured Light, Profile Measurement, Light Plane Calibration, Center Line Extraction.

Abstract: More than 40,000 kilometers of high-speed railway has been built in China, and it is the longest all over the world. The wear of railway rails would affect the safety of train operation. The traditional manual contact measurement methods had the disadvantages of low measurement efficiency and the surface of the measured object was easy to wear. Then, it was of great significance to develop high-precision, non-contact rail profile measurement methods. This paper designed and implemented a method for rail profile measurement with line-structured light. A structured light plane parallel to the cross-section of the rail was emitted by a line laser. The image data were collected by an industrial camera, and then the actual rail profile was extracted through the center line extraction algorithm and coordinate transformation. The method has been tested on 60kg rail profile measurement and the profile measurement experiment results proved it has higher precision and faster speed, compared with results from the Coordinate Measuring Machine (CMM).

1 INTRODUCTION

In recent years, high-speed railways construction in China has developed rapidly and the total operating mileage has exceeded 40,000 kilometers. The high-speed railway network spans north-south and east-west, connecting different cities closely. It greatly meets the travel needs of people and promotes economic development of passing regions and plays an increasingly important role in social development (Ye, 2018). As an important part of the railway system, rail is in direct contact with the train. Severe wear, corrosion, fracture, peeling and other defects will lead to serious safety accidents. Therefore, regular inspection of rails is required. Since the rail profile directly reflects the degree of rail defects and represents the contact condition between wheel and rail, it is necessary to measure the profile of the rail section precisely, and then the data can provide a scientific reference for rail maintenance (Wang et al., 2018).

The traditional rail profile measurement technology mainly depends on measurement tools including mechanical rail wear rulers for contact measurement (Zhang, 2019). Contact measurement requires the participation of inspection personnel, with the disadvantages of a low degree of automation, low testing efficiency, and poor real-time performance, and then it cannot meet the requirements of high-speed railway development (Zhou et al., 2020). Moreover, the contact measurement requires contact with the rail surface, and it will wear instruments, affect the measurement accuracy and damage the surface of the rail (Wu et al., 2020).

By contrast, in the iterative updating process of the computer and electronic technology, the non-contact measurement methods depending on optical means have attracted more attention. They are categorized into passive and active ways according to imaging illumination modes. Passive measurement builds a human-like binocular vision system and it extracts distance information from two different visual directions of a 2D image (Jiang et al., 2020; Xu et al., 2019; Wang et al., 2019). The disadvantages are heavy computing burden, low precision, and slow calculation, and it is highly dependent on the texture characteristics of the measured objects. The active measurement relies on structured light technology. Structured light is categorized into three types based on the beam emitted by the laser: point, line, and plane (Zhang,

Luo, Q., Zhang, S. and Chen, Z.
Line Structured Light Measurement System, Method and Experiments for Rail Profile.
DOI: 10.5220/0011916900003612
In *Proceedings of the 3rd International Symposium on Automation, Information and Computing (ISAIC 2022)*, pages 162-168
ISBN: 978-989-758-622-4; ISSN: 2975-9463

2018). The device of point structured light is simple. However, the shortcomings are cumbersome and time-consuming and not suitable for large-sized objects (Cui, 2018). The surface structured light increases the measurement range and processing efficiency. And the disadvantages are increasing of calibration complexity and data processing. Moreover, since the measurement results are easily affected by the other light sources and the reflection performance of the object surface, it has higher requirements for the measurement environment conditions (Landmann et al., 2018). Compared with the above two types of structured lights, line structured light only uses the emitted light plane to intersect the contour of the object for measurement. The advantages are simple structure, fast image processing speed, and little influence due to environmental conditions, and it has good stability in industrial applications (Lian et al., 2019). For example, it is applied to measure the contour of the disc cam (Hu, 2020) and to the detection system (Ren, 2021).

This paper designed a monocular line structured light rail profile measurement method with the advantages of non-contact, high precision, and high speed. The method first used a line laser to emit a structured light plane parallel to the cross-section of the rail, then collected image data through an industrial camera, and finally obtained the actual rail profile through a center line extraction algorithm and coordinate transformation model. The method has the characteristics of simple equipment and quick processing.

2 METHODOLOGY

In this paper, the monocular line structured light is exploited to realize rail profile measurement. The measurement system schematic diagram is shown in figure 1. The main equipment includes an industrial camera, a line laser, and a computer. The line laser emits a structured light plane parallel to the cross-section of the rail. It forms a structured light band and then the rail profile information is captured on the rail surface. The industrial camera and structured light plane form a certain angle to capture the light band image and then the image is transmitted to a computer. The laser center line of the rail profile image is processed by the corresponding algorithm and the 2D image coordinates are transformed into actual physical coordinates with the camera calibration transformation model. The measurement profile is finally obtained.

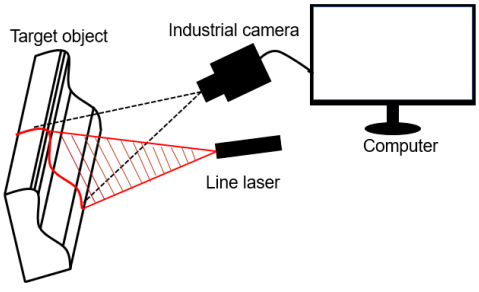

Figure 1: The schematic diagram of the measurement system for the rail profile.

Figure 2 presents the flowchart of the measurement system for rail profile and it consists of four parts: calibration of camera parameters, extraction of profile center line, calibration of light plane parameters, and coordinate transformation. The camera calibration is to obtain the mapping relationship of the image coordinate, camera coordinate, and world coordinate. The extraction of the profile center line mainly realizes rail profile extraction from the image. The calibration of the light plane is applied to obtain coefficients of the structured light plane and then applied for subsequent restoration of the rail profile. The coordinate transformation finishes transforming the 2D profile image into the actual measured profile of the rail.

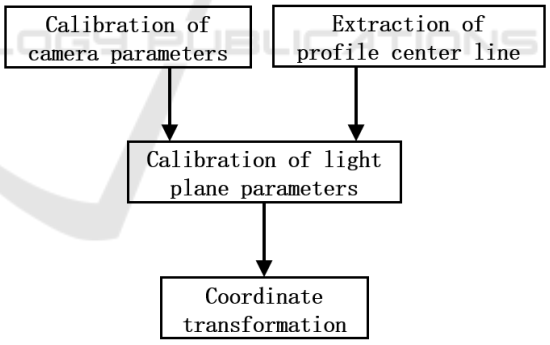

Figure 2: The flowchart of the measurement system.

2.1 Calibration of Camera Parameters

The camera parameters should be calibrated before imaging. In our experiments, a 2D plane calibration plate is applied to the camera calibration. The reason is that a 2D target can provide more reliable manufacturing accuracy and is easy to use, compared with a 3D target.

The world coordinate of the point is represented as $p_W\left(X_W, Y_W, Z_W\right)$, and the pixel coordinate is

represented as $p(u,v)$. Z_C is the scale factor. H is the camera's external parameter matrix and the internal parameters under different spatial poses are represented by matrix M. The camera calibration transformation model is established as equation (1).

$$Z_C\begin{bmatrix} u \\ v \\ 1 \end{bmatrix} = \begin{bmatrix} f_x & \gamma & u_0 & 0 \\ 0 & f_y & v_0 & 0 \\ 0 & 0 & 1 & 0 \end{bmatrix}\begin{bmatrix} R & T \\ 0^T & 1 \end{bmatrix}\begin{bmatrix} X_W \\ Y_W \\ Z_W \\ 1 \end{bmatrix} = MH\begin{bmatrix} X_W \\ Y_W \\ Z_W \\ 1 \end{bmatrix} \quad (1)$$

The parameters to be calibrated are listed in Table 1. The horizontal and vertical scale factors of the image are represented by f_x and f_y, the coordinates of the main point of the image are represented by u_0 and v_0, and γ is the tilt factor. The distortion parameters of the lens are represented by vector K, and the radial and tangential distortion coefficients are represented by ki and pi. The rotation and translation matrix from camera coordinates to world coordinates are represented by R and T, which form the camera external parameter matrix H.

Table 1: The calibration parameters of the camera.

Parameters	Expression
Perspective transformation matrix	$M = \begin{bmatrix} f_x & \gamma & u_0 & 0 \\ 0 & f_y & v_0 & 0 \\ 0 & 0 & 1 & 0 \end{bmatrix}$
Len distortion parameter matrix	$K = \begin{bmatrix} k1 & k2 & p1 & p2 \end{bmatrix}^T$
Rotation matrix	$R = \begin{bmatrix} r_{11} & r_{12} & r_{13} \\ r_{21} & r_{22} & r_{23} \\ r_{31} & r_{32} & r_{33} \end{bmatrix}$
Translation vector	$T = \begin{bmatrix} t_x & t_y & t_z \end{bmatrix}$

2.2 Extraction of Profile Center Line

An ideal structured light image consists of a constant background and a uniform target light band. To calculate the center points of the light band, it is necessary to separate the background from the target light band. However, the unavoidable existence of noise in actual collected images comes from the external environment and inside of the laser. Complex object surface conditions and other factors will bring difficulties to the extraction of the light band, so some actions need to be taken to reduce these bad effects. In this paper, the collected image is pretreated by background processing, Gaussian filtering, and grayscale segmentation. Then the center point is extracted from the target light band by the Steger algorithm. Finally, the image coordinates are restored to real profile coordinates through the line structured light measurement model.

In the step of background processing, two images of the calibration plate are captured when the line laser is working or non-working. These two images are subtracted and then a structured light image with a completely black background is calculated.

After background processing, Gaussian filtering is applied. Gaussian kernel function takes the weighted average results of the gray value of all pixels in the neighborhood to be the gray value of the central pixel. Different weights are set to pixels at different positions and a higher weight is set when the position is closer to the central pixel. Then, it has the advantage that the gray distribution characteristic of the image can be preserved as completely as possible when reducing noise.

Following that, grayscale segmentation is applied. The filtered image can be divided into the light band and background based on the grayscale feature. Assuming that the grayscale of any pixel of the target image is $f(x,y)$, we set a threshold G, and the pixels whose grayscale value is greater than G belong to the foreground, otherwise, these pixels belong to the background.

Then, the Steger algorithm is performed to obtain the center line. It performs Taylor polynomial expansion on the gray distribution of the light band in the normal direction of each pixel and takes the extreme point that satisfies both the polynomial and second derivative of the gray level as the center point of the light band. Compared with other center extraction algorithms, the Steger algorithm has the advantages of better processing accuracy and robustness, and it fully considers the direction of the light band.

According to Steger's conclusion, σ of the Gaussian kernel function should satisfy equation (2).

$$\sigma \geqslant w/\sqrt{3} \quad (2)$$

where w is half of the width of the light band and the scale of the Gaussian kernel function is $3\sigma + 1$.

2.3 Calibration of Light Plane Parameters

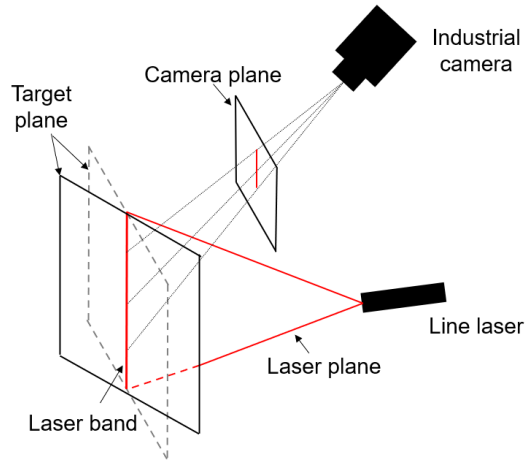

Figure 3. The model of laser plane calibration.

A 2D plane target is adopted in the calibration of the light plane. First, take all points on the light band as a set of calibration points. Second, by freely moving the plane target within the measurement range of the laser, the image coordinates of multiple sets of non-collinear calibration points are obtained. Then convert them into a camera coordinate system according to the relationship between the target plane and the image plane. Finally, the parameters of the light plane are obtained by least squares fitting. We use a 2D calibration plate. During the calibration process, the calibration plate does not need to keep parallel movement and can freely change position and posture within the camera view, reducing the difficulty of operation. There is no need to extract calibration points. We convert all coordinates on the light band to a world coordinate system, which increases the number of calibration points, thereby reducing the error of results.

The specific calibration process is as follows.

(1) The target position is adjusted to locate in the center of the camera view and it is intersected with the structured light plane.

(2) The laser switch is turned on and then the line structured light is emitted to the 2D target. The image is collected. Then the laser switch is turned off without changing the position of the target. Another image is collected.

(3) The position of the target is adjusted and the above steps are repeated to obtain multiple sets of target images and corresponding images with a structured light band.

(4) After completing the above acquisition process, the rotation and translation matrices are calculated by using the perspective transformation matrix M and the model in Section 2.1.

(5) The sub-pixel center points of laser bands of targets with different poses are obtained through image processing algorithms.

(6) Substitute the pixel coordinates of each center point into equation (1) in Section 2.1 to calculate its coordinates $\begin{pmatrix} X_W & Y_W & Z_W \end{pmatrix}$ in target plane world coordinates. The coordinates $\begin{pmatrix} X_C & Y_C & Z_C \end{pmatrix}$ are calculated by equation (3).

$$\begin{bmatrix} X_C \\ Y_C \\ Z_C \\ 1 \end{bmatrix} = \begin{bmatrix} R & T \\ 0^T & 1 \end{bmatrix} \begin{bmatrix} X_W \\ Y_W \\ Z_W \\ 1 \end{bmatrix} = \begin{bmatrix} h_{11} & h_{12} & h_{13} & h_{14} \\ h_{21} & h_{22} & h_{23} & h_{24} \\ h_{31} & h_{32} & h_{33} & h_{34} \\ h_{41} & h_{42} & h_{43} & h_{44} \end{bmatrix} \begin{bmatrix} X_W \\ Y_W \\ Z_W \\ 1 \end{bmatrix} \tag{3}$$

Finally, the light plane is fitted by the least square method.

$$aX_C + bY_C + cZ_C + d = 0 \tag{4}$$

2.4 Coordinate Transformation

Coordinate transformation transforms the two-dimensional pixel coordinates of the center points in Section 2.2 into 3D coordinates of the actual rail profile. It rotates the structured light plane to be parallel to the coordinate plane, and the actual profile curve is calculated.

$$\begin{cases} u - u_0 = f_x \dfrac{X_C}{Z_C} \\ v - v_0 = f_y \dfrac{Y_C}{Z_C} \end{cases} \tag{5}$$

Firstly, the two-dimensional pixel coordinates of the rail profile are taken into equation (5) and three-dimensional coordinates $\begin{pmatrix} X_C & Y_C & Z_C \end{pmatrix}$ of the measurement profile can be obtained with equation (4) in Section 2.3.

Then, the camera coordinates are taken into equation (8) to rotate around the x and y axes and the rotation angle is determined by equations (6) and (7).

$$\begin{cases} \cos\theta = \dfrac{c}{\sqrt{b^2+c^2}} \\ \sin\theta = \dfrac{b}{\sqrt{b^2+c^2}} \end{cases} \tag{6}$$

$$\begin{cases} \cos\varphi = \dfrac{\sqrt{b^2+c^2}}{\sqrt{a^2+b^2+c^2}} \\ \sin\varphi = \dfrac{a}{\sqrt{a^2+b^2+c^2}} \end{cases} \tag{7}$$

$$\begin{bmatrix} X_D \\ Y_D \\ Z_D \end{bmatrix} = \begin{bmatrix} \cos\varphi & 0 & -\sin\varphi \\ 0 & 1 & 0 \\ \sin\varphi & 0 & \cos\varphi \end{bmatrix} \begin{bmatrix} 1 & 0 & 0 \\ 0 & \cos\theta & -\sin\theta \\ 0 & \sin\theta & \cos\theta \end{bmatrix} = R_y R_x \begin{bmatrix} X_C \\ Y_C \\ Z_C \end{bmatrix} \tag{8}$$

After coordinate transformation, the structured light plane is rotated to be parallel to the XOY plane and the actual rail profile coordinates $\left(X_D \ Y_D \ Z_D \right)$ are extracted.

3 EXPERIMENTS AND RESULTS

The BFS-U3-13Y3M black and white area array industrial camera and the Tamron M112FM25 low-distortion industrial lens were used in the experiments. A high-precision checkerboard calibration board with 12x9 corner points was selected and the cell size was 15x15mm. The calibration toolbox Camera Calibrator was applied to the industrial camera calibration in our experiment.

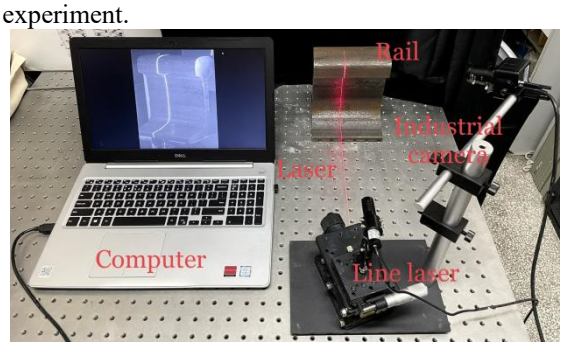

Figure 4. Line structured light measurement system.

The calibration results of the camera are shown in Table 2.

Table 2: The results of camera parameters calibration.

Parameters	Value
Internal parameters	$M = \begin{bmatrix} 5330.6577 & 0 & 640.8603 & 0 \\ 0 & 5330.4521 & 528.7524 & 0 \\ 0 & 0 & 1 & 0 \end{bmatrix}$
Distortion parameters	$K = \begin{bmatrix} 0.0969 & -4.6270 & 0 & 0 \end{bmatrix}^T$

Figure 5(a) presents the line structured light profile image of the 60Kg rail collected in a laboratory environment and Figure 5(b) illustrated the results after center line extraction. Figure 6 provides the visualization results of the center points of the light band in the light plane transformed from local world coordinate systems. The light plane is fitted by the least square method and the values of the parameters are shown in Table 3.

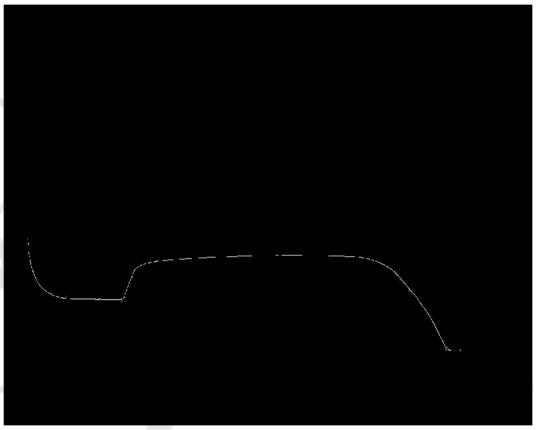

(a) Profile measurement of 60Kg rail.

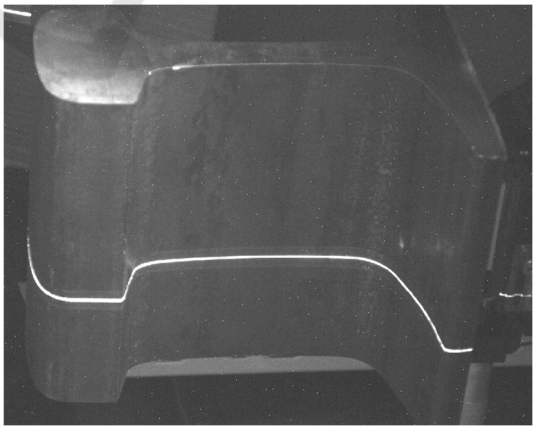

(b) Center line of 60Kg rail.

Figure 5: Images of rail profile.

Table 3: The fitting results of line structure light plane.

Parameters	a	b	c	d
Value	0.1458	-1.4166	-1	962.7770

Figure 7(a) and (b) present the rail profile results between the standard and our measured profiles, and the results between the standard and CMM measured profile, respectively.

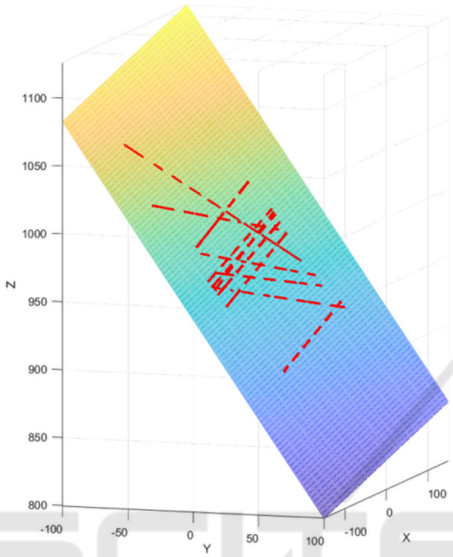

Figure 6: Line structure light plane.

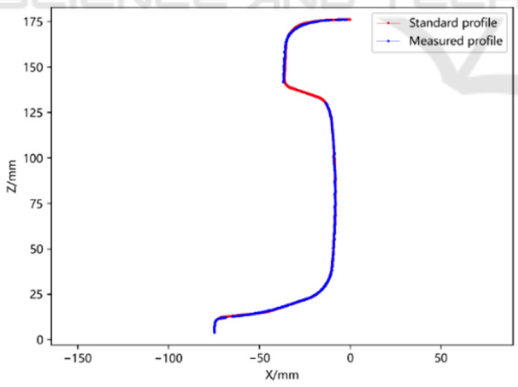

(a) The rail profile measured between the standard and our measured profile.

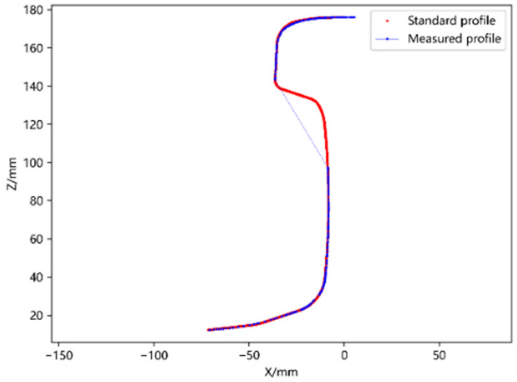

(b)The rail profile measured between standard and CMM measured profile.

Figure 7: The results of measurement.

To quantitatively evaluate the experimental results, three different distance algorithms, including Hausdorff Distance (HD), Frechet Distance (FD) (Alt, 2009; Xie et al., 2017), and Dynamic Time Warping Distance (DTWD) (Keogh et al., 2005) were applied to calculate the fitting degree of rail profile. As shown in Table 4, the results of these distance algorithms proved that our system has higher accuracy compared with CMM.

Table 4: The fit degree of the rail profile (Lower is better for all distance algorithms).

Name	FD	HD	DTWD
CMM	22.71	2.15	0.43
Our	**8.79**	**0.65**	**0.38**

Our measurement method is composed of several different techniques and which are photography, optics, and image processing. The factors affecting measurement error come mainly from two aspects: hardware system and software algorithm.

The error in the hardware system comes from the camera and laser. The camera is used for image acquisition. Higher camera resolution results in less distortion, better performance, higher quality images, and more accurate measurement. The laser is used to emit a line laser. The thinner and straighter the laser is, the better quality of extracted center line will be.

The error in the software algorithm comes from calibration and image processing. The extraction accuracy of calibration points has a great influence on the final results. In our method, all points of the light band are used to fit to reduce the error. Moreover, the extraction accuracy of center points is greatly affected by external noise, the performance of the processing algorithm, and the state of the rail

surface. The background processing algorithm applied in this paper can reduce the errors during processing.

4 CONCLUSION

This paper designed and implemented a method for measuring the profile of rail with a monocular line structured light system. We applied it to measure the 60kg rail profile and compared the results with that from the CMM. The experiment proved that our measurement results are as good as the CMM and our method has higher measurement efficiency compared with the point-by-point contact measurement of CMM. The experiments were completed in a static environment in the laboratory, and further research should focus on profile measurement under outdoor dynamic conditions.

ACKNOWLEDGMENTS

We would like to thank the support from Dr. Peng Wang and Dr. Ji Deng for building the system and data calibration. This research was supported by National Engineering Laboratory for Digital Construction and Evaluation Technology of Urban Rail Transit (grant No. 2021ZH04).

REFERENCES

Ye, H. (2018). Research on key technologies of automatic 3D measurement of high speed railway hub based on line laser scanning. Master's thesis, HUST.

Wang, H., Li, Y., Ma, Z., Zeng, J., Jin, T., and Liu, H. (2018). Distortion rectifying for dynamically measuring rail profile based on self-calibration of multiline structured light. In *IEEE Transactions on Instrumentation and Measurement,* pages 678-689. IEEE.

Zhang, Z. (2019). Research on the rail wear measurement system based on machine vision. Master's thesis, BJTU.

Zhou, Z., Yang, H., and Liu, J. (2020). Research on the three-dimensional detection system of the rail full profile. In *Journal of Physics: Conference Series*, 1633(1): 012002.

Wu, F., Dou, H., Wu, Y., Li, Z., and Yang, X. (2020). Method for detecting sharp rail contour based on machine vision. In *Optical Technique,* 46(04): 453-460.

Jiang, Y., Wang, Z., Han, J., Jin, Y., and Li, B. (2020). Regional fuzzy binocular stereo matching algorithm based on global correlation coding for 3D measurement of rail surface. In *Optik,* 207: 164488.

Xu, G., Chen, J., Li, X., and Su, J. (2019). Profile measurement adopting binocular active vision with normalization object of vector orthogonality. In *Scientific Reports,* 9(1): 1-13.

Wang, P., Li, W., Li, B., and Li, B. (2019). Structured-light binocular vision system for dynamic measurement of rail wear. In *2019 IEEE 2nd International Conference on Electronics Technology (ICET),* pages 547-551. IEEE.

Zhang, S. (2018). High-speed 3D shape measurement with structured light methods: A review. In *Optics and Lasers in Engineering,* 106: 119-131.

Cui, H., Hu, Q., and Mao, Q. (2018). Real-time geometric parameter measurement of high-speed railway fastener based on point cloud from structured light sensors. In *Sensors,* 18(11): 3675.

Landmann, M., Heist, S., Brahm, A., Schindwolf, S., Kühmstedt, P., and Notni, G. (2018). 3D shape measurement by thermal fringe projection: optimization of infrared (IR) projection parameters. In *Dimensional Optical Metrology and Inspection for Practical Applications VII,* 10667: 9-18.

Lian, F., Tan, Q., and Liu, S. (2019). Block thickness measurement of using the structured light Vision. In *International Journal of Pattern Recognition and Artificial Intelligence,* 33(01): 1955001.

Hu, Z. (2020). Research on vision measurement technology of disc cam based on line structure light. Master's thesis, JLU.

Ren, J. (2021). Based on line structured light of pantograph slide abrasion detection system research. Master's thesis, NYCU.

Alt, H. (2009). The computational geometry of comparing shapes. In *Efficient Algorithm*s. pages 235-248.

Xie, D., Li, F., and Phillips, J, M. (2017). Distributed trajectory similarity search. In *Proceedings of the VLDB Endowment,* 10(11): 1478-1489.

Keogh, E., Ratanamahatana, C, A. (2005). Exact indexing of dynamic time warping. *Knowledge and information systems*, 7(3): 358-386.